Journal Pre-proof

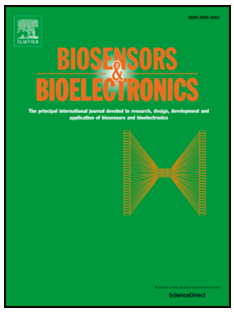

Laser-induced graphene interdigitated electrodes for label-free or nanolabel-enhanced highly sensitive capacitive aptamer-based biosensors

Ajay Kumar Yagati, Arne Behrent, Sebastian Beck, Simone Rink, Achim M. Goepferich, Junhong Min, Min-Ho Lee, Antje Baeumner

PII: S0956-5663(20)30267-0

DOI: https://doi.org/10.1016/j.bios.2020.112272

Reference: BIOS 112272

To appear in: *Biosensors and Bioelectronics*

Received Date: 30 January 2020

Revised Date: 7 April 2020

Accepted Date: 2 May 2020

Please cite this article as: Yagati, A.K., Behrent, A., Beck, S., Rink, S., Goepferich, A.M., Min, J., Lee, M.-H., Baeumner, A., Laser-induced graphene interdigitated electrodes for label-free or nanolabel-enhanced highly sensitive capacitive aptamer-based biosensors, *Biosensors and Bioelectronics* (2020), doi: https://doi.org/10.1016/j.bios.2020.112272.

CRediT author statement

Ajay Kumar Yagati: Conceptualization, Methodology, Validation, Formal analysis, Investigation, Writing - original draft.

Arne Behrent: Methodology, Software, Formal Analysis,

Sebastian Beck: Investigation, Data Curation, Formal Analysis

Simone Rink: Investigation, Data Curation, Formal Analysis

Achim M. Goepferich: Resources, Writing - Review & Editing,

Junhong Min: Supervision, Funding acquisition, Writing - Review & Editing

Min-Ho Lee: Supervision, Funding acquisition, Writing - Review & Editing,

Antje Baeumner: Conceptualization, Methodology, Resources, Writing - review & editing, Supervision, Project administration, Funding acquisition.

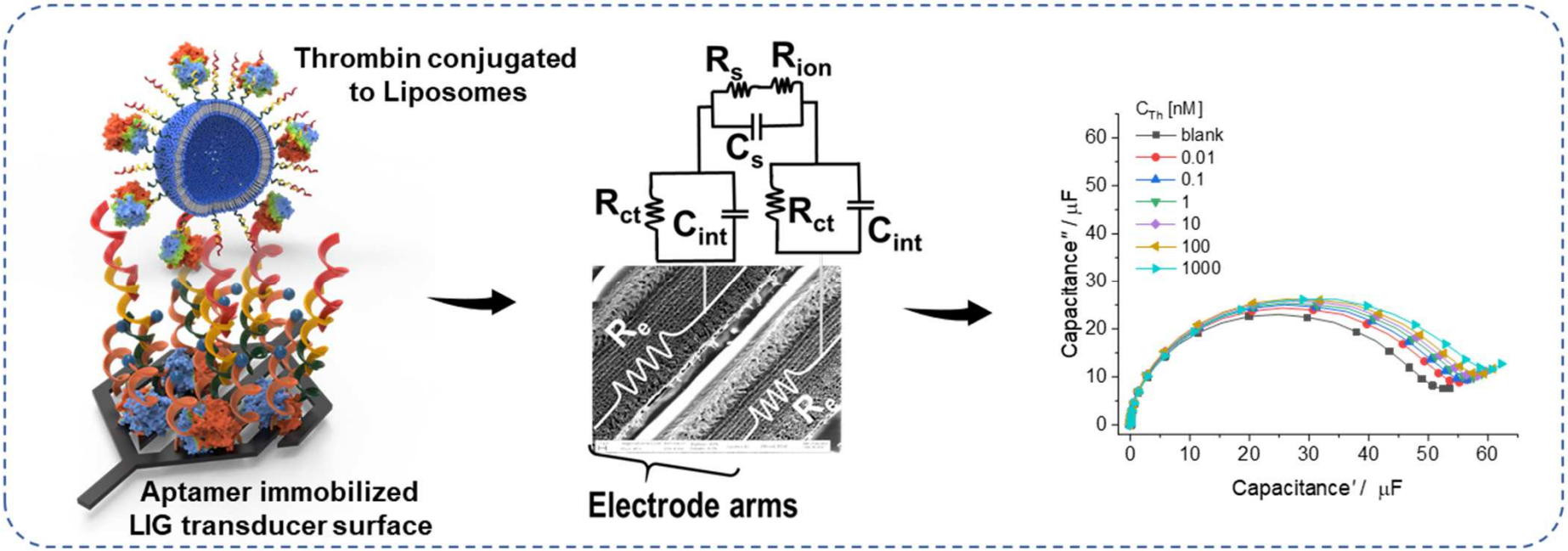
Thrombin conjugated
to Liposomes
Aptamer immobilized
LIG transducer surface
R_s
R_{ion}
C_s
R_{ct}
C_{int}
R_{ct}
C_{int}
R_e
R_e
Electrode arms
C_{Th} [nM]
blank
0.01
0.1
1
10
100
1000
Capacitance″ / μF
Capacitance′ / μF
0
10
20
30
40
50
60

Laser-induced graphene interdigitated electrodes for label-free or nanolabel-enhanced highly sensitive capacitive aptamer-based biosensors

Ajay Kumar Yagati[1,2], Arne Behrent[1], Sebastian Beck[3], Simone Rink[1], Achim M. Goepferich[3], Junhong Min[2,*], Min-Ho Lee[2,*], Antje Baeumner[1,*]

[1] *Institute of Analytical Chemistry, Chemo-and Biosensors, Faculty of Chemistry and Pharmacy, University of Regensburg, 31, 93053, Regensburg, Germany*

[2] *School of Integrative Engineering, Chung-Ang University, Heukseok-dong, Dongjak-Gu, 06974, Seoul, Republic of Korea*

[3] *Department of Pharmaceutical Technology, Faculty of Chemistry and Pharmacy, University of Regensburg, 93040 Regensburg, Germany*

***Corresponding Author**

Antje J. Baeumner
Email: antje.baeumner@ur.de; Tel: +49-941-943-4066; Fax: +49-941-943-4064

Junhong Min
Email: junmin@cau.ac.kr; Tel: +82-2-820-5348; Fax: +82-2-814-2651

Min-Ho Lee
Email: mhlee7@cau.ac.kr; Tel: +82-2-820-5503; Fax: +82-2-814-2651

Abstract

Highly porous laser-induced graphene (LIG) is easily generated in complex electrode configurations such as interdigitated electrodes (IDEs). Here, we demonstrate that their superior capacitive response at low frequencies can be exploited in affinity biosensors using thrombin aptamers as model biorecognition elements. Of specific interest was the effect of electrode surface area on capacitance detection, and the comparison between a label-free format and enhancement strategies afforded by carboxy group bearing polymeric nanoparticles or liposomes. Electrochemical impedance spectroscopy (EIS) was used to investigate the LIG performance and optimize the biosensor design. Interestingly, the label-free strategy performed extremely well and additional labels decreased the limit of detection or increased the sensitivity only minimally. It is assumed that the highly porous nature of the LIG structures dominates the capacitive response so that labels removed from the surface have only limited influence Also, while slight performance changes can be observed for smaller vs. larger electrode structures, the performance of a LIG IDE is reasonably independent of its size. In the end, a dynamic range of 5 orders of magnitude was obtained (0.01 nM – 1000 nM) with a limit of detection as low as 0.12 pM. When measured in serum, this increased to 1.3 pM. The good reproducibility (relative standard deviation (RSD), 4.90 %) and repeatability (RSD, 2.59 %) and good long-term stability (>7 weeks at 4 °C) prove that a LIG-based capacitance sensor is an excellent choice for affinity-based biosensor. The ease-of-production, the simplicity of modification and the superior performance even in a label-free format indicate that LIG-based biosensors should be considered in point-of-care diagnostics in the future.

Keywords: Aptamer; liposomes; interdigitated electrodes; nanoparticles; impedance; capacitance; laser-induced graphene.

1. Introduction

Thrombin (MW: 37.4 kDa) a two-polypeptide chain, glycosylated serine protease is composed of two anion binding exosites which complexes with fibrinogen and heparin (Esmon and Lollar 1996). Thrombin plays a vital role in hemostasis and hemolysis that may lead to vascular and endothelial dysfunctions, it is considered a tumor marker in pulmonary metastasis and increased concentrations in blood lead to the associated diseases. Under normal conditions, thrombin is not found in blood, however, its inactive form, prothrombin, is present at a level of 1.2 µM (Deng et al. 2014). Quantitative determination of thrombin has become a routine tool for early diagnosis, monitoring, and estimation of hematological system disorders, making the availability of a simple biosensor that covers the required dynamic range 1-500 nM (Wolberg and Campbell 2008) and offers ultra-low limits of detection such as in the low pM range (Li et al. 2019).

Aptamers are well-known and accepted biorecognition elements in biosensors as they can possess a high affinity to specific targets (Bin Seo and Gu 2017) and are much easier synthesized and produced than the traditionally used antibodies. Aptamers for thrombin detection are prime examples, with its two most often used sequences, a 15-mer and a 29-mer, binding to two different electropositive exosites of the thrombin (Edwards et al. 2010). They have consequently been used as biorecognition elements in a variety of approaches including fluorescence (Duan et al. 2015), electrochemical (Grabowska et al. 2018), colorimetric(Zhao et al. 2007) and surface plasmon resonance (Zhu et al. 2015) strategies. Interestingly, electrochemical-based aptamer detection systems were found to provide the lowest limits of detection paired with better sensitivity. Ideal biosensors should furthermore enable straightforward detection without additional labeling steps, be inexpensive and simple in their production and not be only minimally affected by a sample matrix. We were therefore

interested in studying label-free capacitive sensing strategies with laser-induced graphene (LIG) electrodes (Griffiths et al. 2014). In addition to enabling ultra-easy fabrication through a simple CO_2-laser printer these electrodes are highly porous with fast heterogeneous electron transfer rates and numerous possibilities of chemical functionalization (Fenzl et al. 2017). They hence lend themselves extremely well to pursue the common strategies to improve a biosensor's sensitivity such as by adopting porous/nanostructured electrode materials, with innovative electrode design structures (Yagati et al. 2016), labeling methods (Sun et al. 2019), and rational design of surface chemistry (Campuzano et al. 2019). In the following, recent literature on using LIG electrodes as a signal-transducing and sensing material for electrochemical sensing is reviewed. (Nayak et al. 2016) adopted LIG electrodes for improved electrocatalytic activity toward oxidation of ascorbic acid (AA), dopamine (DA), and uric acid (UA), similarly (Xu et al. 2018) also developed an electrochemical sensor for neurotransmitter with a LOD of 0.43 µM. Furthermore, photoelectrochemical applications on LIG electrodes were performed (Ge et al. 2019a; Ge et al. 2019b) for AA detection with a stable photoelectrochemical response under visible light with an LOD of 5.4 pg/mL. However, many of the previously reported literature have one or some of the short comings: i) they have long turnaround time to provide results ii) the LOD's are still high in µM range, iii) more importantly, there is a lack of surface engineering to bind the analyte molecules. Non-faradaic EIS may become a superior detection method for point-of-care-testing (POCT) applications. Its ability to detect only molecular surface events rather than also those taking place in the bulk solution, makes it superior to voltammetric approaches. In the case of photoelectrochemical approaches, the additional hardware requirements make it less advantageous as POCT system.

Therefore, capacitive approaches derive from impedance spectroscopy affording high sensitivity in a label-free format (Nguyen et al. 2018). The principle of capacitive biosensors

is based on the change in the electrical surface or thickness of the dielectric layer on the electrode surface. The working electrode immobilized with receptor molecules possesses a stable capacitance, and subsequent binding with a target analyte will cause changes in capacitance (Tsouti et al. 2011). In relation with the present work, these capacitive changes can be analyzed as the complex impedance $Z^*(\omega)$ function can be converted into a complex capacitance $C^*(\omega)$ by the physical definition $Z^*(\omega)=1/j\omega C^*(\omega)$ in which ω is the angular frequency (Fernandes et al. 2013). These plots provide an intuitive way of interpreting the impedance spectroscopy of an electrochemical capacitor and evaluate the total specific capacitance and time constant (Randriamahazaka and Asaka 2010). Thus, recently, several capacitive biosensors have been reported for the detection of NS1 biomarker (Cecchetto et al. 2017), bacteria (Erturk and Lood 2018), HIV-1 p24 (Teeparuksapun et al. 2010), insulin (Yagati et al. 2016).

Thus, in the present work, LIG electrodes are investigated in their capability to serve as a capacitance-based transducer. The effect of the electrode surface area, of label-free and two different nano-label approaches were studied and applied as aptamer-biosensors for the detection of thrombin in buffer and serum samples (Figure 1).

2. Materials and methods

2.1. Chemicals and reagents

The polyimide foil for the LIG IDE electrodes was purchased at Dasom RMS Co. LTD (Seoul, South Korea). 1-Pyrenebutyric acid (PyBA, 97 %), N-(3-Dimethylaminopropyl)-N′-ethylcarbodiimide hydrochloride (EDC, purum, 98%), N-hydroxysuccinimide (NHS, 98%), Dimethyl sulfoxide (DMSO, ≥ 99.9 %), thrombin (from human plasma, ≥ 2,000 NIH units/mg), and fetal bovine serum were obtained from Sigma-Aldrich. Antithrombin aptamers

(*i*) primary with 15 nucleotides (5′-H_2N-C6-GGTTGGTGTGGTTGG-3′) and (*ii*) secondary with 29 nucleotides (5′-H_2N-AGTCCGTGGTAGGGCAGGTTGGGGTGACT-3′) were synthesized and purchased from Eurofins Genomics (Ebersberg, Germany). 2-(N-morpholino) ethanesulfonic acid (MES; 0.1 M, pH 5.5), The phosphate-buffered saline solution (PBS) consisted of 0.1 M phosphate buffer, 1.37 M NaCl, and 0.03 M KCl (pH 6.5). Tris-EDTA (TE) buffer pH 7.5 was used for dissolving the aptamer and consisted of 0.01 M Tris-HCl and 0.001 M EDTA. Ultrapure water (18.2 MΩ/cm) was obtained from an Ultrapure (Milli-Q) system and used throughout. Phospholipids 1,2-dipalmitoyl-sn-glycero-3-phosphocholine (DPPC), 1,2-dipalmitoyl-sn-glycero-3-phospho-(1′-rac-glycerol) (sodium salt) (DPPG), and 1,2-dipalmitoyl-sn-glycero-3-phosphoethanolamine-N-(glutaryl) (sodium salt) (N-glutaryl-DPPE) were purchased from Avanti Polar Lipids, USA, *m*-carboxy luminol (purity: 73.597 wt% ± 2.82 wt%) was customized synthesized, HEPES (4-(2-Hydroxyethyl)piperazine-1-ethane sulfonic acid, purity >99.5 %), chloroform and methanol were purchased from VWR chemicals, Germany. Cholesterol, Sephadex® G 50, sucrose, sodium azide, glycine (purity >99.7 %), sodium hydroxide, Whatman Nucleopore™ Track-Etched membranes 1.0 µm, 0.4 µm, and 0.2 µm, 19 mm diameter were purchased from Sigma Aldrich/Merck, Germany. Dialysis tube Spectra/Por© 4 was obtained from Carl Roth, Germany. All other reagents were of analytical reagent grade or the highest purity available and were used directly without further purification unless indicated otherwise.

2.2. Apparatus

Optical measurements for the IDE electrodes were obtained from the digital microscope (KERN Optics). Field emission scanning electron microscopy (FESEM) images were recorded on Zeiss Leo 1530 scanning electron microscope (Carl Zeiss Microscopy GmbH,

Germany). Dynamic light scattering for size distribution results and zeta potential was recorded on Malvern and Zetasizer. Electrochemical impedance spectroscopy was performed using a frequency response analyzer using PalmSens4 (The Netherlands) scanned in the frequency range of 1 MHz to 0.1 Hz.

2.3. Electrochemical impedance spectroscopy (EIS) measurements

Non-Faradaic EIS measurements were conducted in a two-electrode configuration in PBS (10 mM, pH 6.5) within a frequency range of 0.1 Hz to 100 kHz, an AC waveform of 5 mV, with a dc potential of 0 V applied to minimize any background signal or contributing electric fields. EIS curves were initially plotted in the form of Bode plots, later they were converted to capacitance spectroscopy by converting the complex impedance Z*(ω) to complex capacitance by C*(ω) = 1/$j\omega$Z*(ω), where ω is the angular frequency. The real and imaginary parts could be derived from the complex impedance by the following expressions (Taberna et al. 2003),

$$C'(\omega) = \frac{-Z''(\omega)}{\omega|Z(\omega)|^2} \quad (1)$$

$$C''(\omega) = \frac{Z'(\omega)}{\omega|Z(\omega)|^2} \quad (2)$$

in which, $C'(\omega)$ and $C''(\omega)$ are the real and imaginary parts of the capacitance $C^*(\omega)$ and |Z(ω)| is the impedance modulus. The real part of the capacitance C′(ω) corresponds to the capacitance of the cell measured under low-frequency alternating current conditions, and C″(ω) is the imaginary part of the capacitance corresponding to losses in the form of energy dissipation (Randriamahazaka and Asaka 2010). The obtained impedance results were fitted with proper circuit elements using in-built EIS equivalent circuit analysis software provided by PSTrace 5 using the Levenberg-Marquardt algorithm for the whole spectral range.

2.4. Fabrication of laser scribed graphene interdigitated electrodes

Three electrode sets of interdigitated electrodes (IDEs) having varying number of fingers 16, 10 and 8 having 200 × 200 µm (width (*w*) × spacing (*s*)) size were fabricated on polyimide film using X-660 laser scriber platform (Universal Laser Systems, Scottsdale, AZ, USA) with a wavelength of 10.6 µm. The optimized laser power, speed, pulses per inch (PPI), and the Z-focus distance between laser and the sample were 0.81 W, 5.8 cm s^{-1}, 1000 and 2000 PPI in *x* and *y* direction, and -0.5 mm, respectively. All the laser-induced experiments were performed under ambient conditions. The fabrication procedure of LIG IDEs was shown in supporting information (.mp4 video). After fabrication procedures, the electrodes are cut, passivated and Cu terminal pads were attached for robust EIS measurements (see Figure S1).

2.5. Synthesis of –COOH terminated polymer nanoparticles for thrombin bindings

Nanoparticle preparation procedure was adapted from literature (Abstiens et al. 2019). In brief, nanoparticles were manufactured by already known nanoprecipitation. The organic phase consisted of COOH-PEG5k-PLA10k, MeO-PEG2k-PLA10k, PLGA 13.4k and acetonitrile, which was injected into vigorously stirred Dulbecco´s phosphate-buffered saline (DPBS ×0.1, pH 7.4). Acetonitrile was evaporated for 3 hours. Finally, nanoparticles were washed and concentrated using a Microsep Advance spin filter (Pall Corporation) with an MWCO of 100 kDa (1200 ×g, 15 min).

2.6. Synthesis of –COOH terminated liposomes

Liposomes with 8 % carboxy functionalization on the surface were prepared according to an established protocol (Mayer et al. 2018) with adjustments towards phospholipid composition, containing DPPC (41.9 µM), DPPG (20.3 µM), cholesterol (52.7 µM) and N-

glutaryl-DPPE (9.19 µM) dissolved in a mixture of 3 mL chloroform and methanol. The remainder of the protocol was as previously reported and detailed in the SI.

2.7. Aptamer biochip fabrication

The procedure for attachment of thrombin specific aptamers onto the LIG IDEs was adapted from our earlier reported literature (Fenzl et al. 2017) with minor modifications and the sequential steps followed are shown in Figure 1. Briefly, a bare LIG IDE was first immersed in 10 mM 1-pyrenebutyric acid (1-PyBA) in DMSO for 90 min to form a self-assembled monolayer followed by thorough rinsing with DI water. The 1-PyBA coated electrodes were then covered with a mixture of 50 mM EDC and 100 mM sulfo-NHS solution in 10 mM MES buffer (pH 5.5) for 40 min to form an amine-reactive surface. Next, the electrodes were rinsed with DI water and reacted with10 µM amine-modified thrombin specific aptamer **I** (5′-H_2N-C6-GGTTGGTGTGGTTGG-3′) in an aqueous solution consisting of TE buffer pH 7.5 (0.01 M Tris-HCl and 1 mM EDTA) for at least 3 h in a humidity chamber. The electrodes were rinsed with phosphate-buffered saline (PBS, pH 7) and subsequently, 1% BSA was added onto the electrodes for 1 h to avoid non-specific bindings for the immunoreactions. After washing with DI water, the aptamer chip was stored in the chamber at room temperature. Finally, different amounts of thrombin were dissolved in PBS (pH 6.5) or serum to obtain final concentrations of 0.01 to 1000 nM and were examined with EIS measurements.

2.8. Characterization of liposomes and its conjugations

Dynamic light scattering (DLS) measurements were performed with a 1:100 dilution of liposomes in HSS buffer resulting in an approximate phospholipid concentration of 100 µM. A disposable micro cuvette was filled with 1 ml of the suspension and analyzed with the

particle sizer in the backscattering mode at an angle of 173° (Malvern Zetasizer Ver.7.11) at 25 °C after an equilibration time of 70 s. After 10 consecutive measurements, the Z-average (d.nm) and a polydispersity index (PDI) were extracted from the autocorrelation data. Also, the electrophoretic mobility of the purified liposomes was measured with the same 1:100 dilution of liposomes in HSS buffer. A folded capillary cell (Malvern DTS1070) was filled with ~800 µL of the liposome dispersions and equilibrated to 25 °C for 70 s. The mean electrophoretic mobility was determined by laser Doppler velocimetry with the Zetasizer nano series. The Smoluchowski model was employed to determine the zeta potential of the dispersions (Fenzl et al. 2015).

2.8. Aptamer conjugation with carboxy liposomes (LPs), carboxy polymers NPs (PNPs) for thrombin bindings

Briefly, 100 µL of the carboxy-nanoparticles as prepared in section 2.5 were added with 100-fold molar excess of EDC and NHS mixed with a solution containing 20 µL of 50 mM EDC and 100 mM sulfo-NHS mixture and the reaction mixture was gently vortexed and left for 40 min at 25 °C to form amine-reactive group on the particle surface. Afterward, 10 µL of 10 µM aptamer **II** (5′-H_2N-AGTCCGTGGTAGGGCAG GTTGGGGTGACT-3′) in TE buffer solution was added in a vial and kept for incubation at r.t. (room temperature) for approx. 3 h. Aptamer conjugated polymer particles colloids were finally rinsed by centrifuging (6000 × g, 7 min) and resuspended in 10 mM PBS buffer solution to remove excess aptamers, EDC and unreacted salts. The aptamer conjugation on PNP surfaces then added with different concentrations of thrombin for capacitance measurements. Likewise, the same protocol as described was adopted for the aptamer bindings with liposomes, except the form liposome dilutions were performed in 0.1 M glycine-NaOH pH 8.6 (Osmolality 0.52 osmol/kg) and the

aptamer bound liposomes after 3 h incubation period, each sample solution was subjected to dialysis against deionized water for 2 h using 2000 MWCO (molecular weight cut-off) dialysis tubes to remove unreacted EDC, aptamers, and buffer salts.

3. Results and discussions

3.1. Characterization of LIG IDEs, polymer nanoparticles, and liposomes.

All components of the biosensor were characterized using scanning electron microscopy (SEM) and in the case of the nanoparticles and liposomes also via dynamic light scattering. Top views of the electrodes display the expected highly structured porous carbon film (Fig. 2a), whereas the cross-sectional view (Figure 2b) shows the sheet-like structure of the graphene layer with a thickness of 45 µm. SEM analysis of the carboxy terminated polymer nanoparticles shows uniformly sized particles around 60 nm evenly distributed over the entire surface (Figure 2c) which agrees with the DLS analysis shown in the inset of Fig. 2c. Furthermore, the SEM analysis on the liposomes shows spherical shaped particles formed on the substrate (Figure 2d) and the diameters of the liposomes are consistent with the results of dynamic light scattering (inset of Fig.2d). Observed size variations in the SEM image are likely caused by the drying and staining process.

3.2. Sensing mechanism, sensor structure and characterization of LIG IDEs

Previous research in our group indicated that LIG electrodes demonstrate a surprisingly high performance at low-frequency ranges in electrochemical impedance-based studies with cell monolayers (data not published yet). This finding was exploited here to develop capacitance-based biosensors using aptamers as biorecognition elements. First, various specifications of interdigitated electrodes (IDEs) were fabricated, generally characterized (Fig. 2 and 3) and evaluated as an actual transducer in the biosensing detection of thrombin in PBS and serum

samples (Fig. 4). Specifically, Figure 3(a-c) shows the IDE sensors with the same interdigitated structure of 0.2 × 0.2 mm (width (*w*) × spacing (*s*)), however, with overall different sizes due to changing numbers of electrode arms (16 (electrode 1), 10 (electrode 2), 8 (electrode 3)). When a bare, porous IDE is immersed in an electrolyte solution, neighboring fingers can be approximated by an equivalent model as shown in Figure 1b, indicating mainly four electrochemical processes (Cheng et al. 2016; Ogihara et al. 2015), (*i*) mixed conduction with both electron and ion species as electric resistance (R_e), electrolyte bulk resistance (R_{sol}), and ionic resistance in pores (R_{ion}); (*ii*) interfacial capacitance between electrode and electrolyte (C_{int}) arises from the electric double layer, electrolyte capacitance (C_s); (*iii*) charge-transfer resistance between electrode and electrolyte as R_{ct}; and (iv) mass transfer to compensate for charge as diffusion. Among these parameters, C_{int} is of greatest interest for biosensing strategies as it correlates to molecular depositions and nanostructure morphologies (see Figure S2). Thus, for the given impedance network the equivalent circuit can be simplified as a series connection of two interfacial capacitance (C_{int}) and the combination of ion resistance in pores (R_{ion}) with electrolyte bulk resistance (R_s) (Fig. 1b). Furthermore, since the two C_{int} observed are in series, we can simplify and define the equivalent capacitance as $C_{eq}=C_{int}/2$. It can, therefore, be concluded that the measured impedance on each LIG electrode is $Z_{LIG\text{-}IDE}=R - j/\omega C_{eq}$, where *j* is the imaginary unit ($\sqrt{-1}$), and ω is the angular frequency.

Further, the observed impedance can be fitted to the R-CPE equivalent model, in which the constant phase element (CPE) is defined as

$$CPE = 1 / T(j\omega)^P \quad (3)$$

Here, *j* is the imaginary unit and *T* is equivalent to the capacitance (C_{int}) of a perfect capacitor. The coefficient *P* varies between 0 and 1, where $P = 1$ represents the impedance of

an ideal capacitor. *T* has units of capacitance (F); in case $P < 1$, T has units of $F/s^{(1-P)}$ (Castiello et al. 2019).

The Bode plots (|Z|, ϕ vs. f) of all three types of electrodes were measured when immersed in 10 mM PBS and the obtained spectra were fitted to the model shown in the *inset* of Figure 3d. Additionally, the measured Bode plots were converted into complex capacitance plot (C′ vs C″) by using eq.1 and 2 shown in Figure 3e. From the fitting analysis, the extracted values of -total ionic and solution resistance (R) and the constant phase element (CPE) are given in Table 1. Not surprisingly, a decreased impedance magnitude (|Z|) was observed for electrode 1 in comparison to the higher |Z| for electrode 3, which suggests that electrode 1 possessed more electroactive surface area with a higher mass transport rate. It can also be seen from Figure 3d that at high frequencies (1 MHz to 100 Hz) the capacitive element is negligible, and |Z| is equal to R_s. At lower frequency (100 to 0.1 Hz), the capacitive contributions become much greater than the solution resistance and the overall impedance observed is mainly due to the capacitive behavior of the electrode sensor, which is equivalent to $Z=1/\omega C_{eq}$. The complex capacitance plots enabled better estimation of the electrode capacitance (see Fig. 3e) and show that electrode 1 possessed an almost 3x higher capacitance (110 µF) than electrode 3 (40 µF) when the physical area is only 2× higher. This clearly suggests that the obtained spectra are in a simple correlation of $C = \varepsilon A/d$ (where *A* is the electrode area, ε the permittivity of the medium, and *d* is the distance between the electrode fingers) which also holds true for such highly porous electrode structures. Further studies were performed to examine the electrode sensitivity for their applications in other electrolytes (Figure S2(a,b)). The experimental data were fitted with ([R-CPE]C) equivalent circuit model (Fig. S2(d)) and the extracted values were presented in Figure S2(c). It is noteworthy when both are compared, the smaller electrode is found to be less sensitive as it couldn't show any significant changes for any solvent except 10 mM PBS.

3.3. Characterization of the chemical and biological modification steps of the IDEs

Careful analysis of chemical and biological surface modifications of the IDEs assists in optimizing each single modification step (Fig. S3). Thus, the IDEs were analyzed after each step via EIS in 10 mM PBS pH 6.5 and analyzed using Nyquist (complex capacitance) plots (Fig. 4(a, b)) and corresponding Bode plots (Fig. S4, S5) for both bigger (no. 1) and smaller (no. 3) electrodes. The detection principle of a capacitive biosensor is based on measuring the level of capacitance change between interdigitated electrode pairs induced by the change in dielectric constant (relative permittivity) due to affinity-based electron exchange in between aptamers/antigens and electrodes. The more aptamer-antigens binding occurs, the more capacitance change is measured due to the change in the dielectric constant of the capacitance media. The Nyquist plots of the bare electrodes show the expected semicircle in which the diameter corresponds to the change in capacitance of the electrode and a straight line, which is due to the mass transfer of ions in the low-frequency region caused by the porous nature of the electrode material. 1-Pyrenebutric acid (1-PyBA) films double the overall capacitance due to the highly charged nature of this film. Activation with EDC-NHS forms a less charged amide bond and together with subsequent immobilization procedures with aptamer and BSA, the net capacitance tends to decrease as more and more blockage of the surface occurs. However, upon binding to thrombin, the aptamer folds into a configuration (Cunningham et al. 2014) which sequesters Th, reduces its access to the electrode surface which in turn results in an increase in capacitance. Besides, aptamer carries a negative charge due to the phosphate group (Deng et al. 2014) and, the isoelectric point of thrombin is high, and that thrombin is a cation at the pH of the blood. It was also found that thrombin adsorbs readily to surfaces, especially negatively charged surfaces (Berg et al. 1979).The capacitance change for both bigger (Elec 1) and smaller electrode (Elec 3) upon modifications with SAM layers and

subsequent binding with Th was found for 1-PyBA (68.36, 27.20 µF), EDC/NHS (54.2, 20.2 µF), aptamer (59.0, 18.4 µF), BSA (42.8, 17.6 µF), Th (50.9, 18.3 µF) respectively. Only limited optimization of existing protocols published earlier were needed for the separate modification steps as outlined in the methods section.

DLS measurements (Figure 4c) yielded a size of 156 nm ± 48 nm with a polydispersity index of 0.08 ± 0.01, zeta potential measurements (Figure 4d) yielded a surface charge of -34.9 mV ± 1.8 mV and ICP-OES measurements yielded a phospholipid concentration of 8.9 ± 0.04 mM. The biological modification of both liposomes and nanoparticles was also followed using DLS and zeta potential measurements. The original hydrodynamic diameter of –COOH liposomes (142.8 nm with a polydispersity index (PDI) of 0.08) increased with additional modification with the aptamer (144.7 nm (PDI of 0.084)) and after binding to 1 µM thrombin (146.9 nm (PDI of 0.087)). The original zeta potential of the –COOH-liposomes (−34.2 ± 2.1 mV) decreased indicating the loss of free carboxy groups to −17.6 ± 1.06 mV after aptamer conjugation and −16.02 ±1.02 mV after binding to thrombin. Similarly, the hydrodynamic diameter of the original polymer nanoparticles (60.77 nm (PDI of 0.125)) increased after aptamer modification (62.47 nm (PDI of 0.145)) and binding to 1 µM thrombin (65.83 nm (PDI of 0.187)). Also, the zeta potential followed the expected trend decreasing from the original −10.29 ± 0.31 mV to −8.1 ± 0.38 mV and −8.05 ±0.25 mV.

3.4. Detection of thrombin with its conjugated nanoparticles in PBS and serum

The optimized biosensors were then used for the detection of thrombin in PBS and in serum samples. Here, label-free and label approaches (liposomes and nanoparticles) were compared on the large (Fig. 5a-c) and small IDE transducers (Fig. 5d-f) generating Nyquist capacitive plots for the thrombin concentrations tested ranging from 0.01 to 1000 nM (Figure 5a-f). The capacitive responses obtained from the impedance analysis were linear over the measured

concentration range resulting in an increase of the real part of capacitance (C') with an increasing concentration of thrombin. This phenomenon of change in capacitance is in agreement with earlier reports using the EIS method (Meini et al. 2012). The change in capacitance $\left(\Delta C = C'_{after} - C'_{before}\right)$ (Kuo et al. 2018) was evaluated in more detail (Figure S6) which positively relates to the thrombin concentration for all combinations of measurements. The most significant change in ΔC was observed at 0.5 Hz thus, $\Delta C_{\text{at 0.5 Hz}}$ was recorded after each addition of thrombin to determine the sensor sensitivity and detection limit. Linear fit lines where y is $\Delta C_{\text{at 0.5 Hz}}$ and x is the concentration of thrombin in ng/mL were obtained for all variations, i.e. the small electrode label-free ($y = 0.259x + 3.22$) with nanoparticles as label ($y = 0.395x + 4.67$) or liposomes as label ($y = 0.686x + 8.01$); and the bigger electrode label-free ($y = 0.591x + 7.81$), with nanoparticle ($y = 0.855x + 11.9$) or liposomes ($y = 1.02x + 14.1$). The limit of detection (LOD) was experimentally obtained ($3.3S_b/m$)(Hayashi et al. 2004), and found to be 0.12 pM; where S_b is the standard deviation of the measurement signals on the bare electrode and m is the slope of the analytical curve. All data are summarized in Table 2. It can be seen that (*i*) all the biosensing strategies demonstrate a large dynamic range (5 orders of magnitude), (*ii*) extremely low limits of detection especially when compared to previously developed thrombin sensors (Table 3), (*iii*) and that the addition of labels lowers the LOD and increases the sensitivity, but only minimally. It is assumed that the highly porous nature of the LIG structures dominates the capacitive response so that labels removed from the surface only have limited influence (*iv*) The difference between results obtained by larger and smaller IDE structures is also minimal. It can be concluded that the LIG IDEs are very well suited for capacitive sensing and can be adapted in size to the experimental set-up needed.

The clinical applicability of the sensor was investigated by determining thrombin in undiluted fetal bovine serum samples using aptamer immobilized on the larger electrode design (no. 1). Different concentrations of thrombin (0.01 to 1000 nM) were spiked into serum and applied to the sensor (Figure S7(a,b)). As can be seen, when compared to calibration plots obtained from analysis in PBS, minimal matrix effects are observed which is due to the BSA blocking step included in the IDE surface modification (Figure 6c). The response found was linear with a regression equation of $y = 0.611x + 7.68$; R^2=0.990 (x: nM, y: $\Delta C_{at\ 0.5\ Hz}$); with a LOD estimated to be 1.3 pM, which is only 10x higher than the best LOD determined in PBS and below the required clinical of 1 nM (Wolberg and Campbell 2008).

3.5. Stability and reproducibility of the LIG IDEs for practical applications

In order to examine the selectivity of the sensor, negative control experiments were performed using electrodes missing the anti-thrombin aptamer (i.e. BSA/1-PyBA/IDEs). Again, different thrombin concentration was incubated with the sensors resulting in no measurable change in capacitance. For long-term stability studies, the BSA/Aptamer/1-PyBA/IDE electrodes were kept at 4 °C in 10 mM PBS in a humid chamber after each impedance measurement. Surprisingly, the electrode retained ~98% of its initial response even after 7 weeks, indicating a highly robust biosensor structure. In addition, reproducibility (expressed as the % relative standard deviation (% RSD) of repetitive measurements (n=5) of the developed thrombin immunosensor was examined. The intra-assay precision of the immunosensor was examined by detecting 1 µM thrombin in three replicate measurements, whereas the inter-assay precision was evaluated by measuring 10 µM of thrombin in three independently prepared BSA/Aptamer/1-PyBA/IDEs. The intra- and inter-assay RSD were found to be 4.9 % and 2.6 % respectively, thereby indicating acceptable levels of precision and reproducibility.

4. Conclusion

By developing high-quality LIG electrodes for capacitance-based detection of thrombin in complex biological matrices, we could clearly demonstrate that these novel electrodes are extremely well suited for such challenging bioanalytical strategies. Their excellent surface qualities, i.e. graphene-like material and high inherent porosity, enable superb capacitive sensing in the low-frequency range and result in ultralow limits of detection without the need for additional labels. In fact, it is assumed that the overall sensitivity of the electrode observed by C_{eq} is mainly influenced by the porosity of the electrode as only little contributions from the nanolabels were observed. Interestingly, these LIG characteristics important for capacitive sensing are not influenced by geometrical parameters such as electrode size and therefore allow for highly flexible biosensor and bioassay design.

LIGs have been used already in voltammetric detection strategies, similarly, taking advantage of the large inherent electrode surface area. However, our simple, label-free capacitive strategy offers better limits of detection than amperometric detection of thrombin on porous electrode surfaces (Sun et al. 2014) or those with graphene oxide as an enhancer (He et al. 2014). It can thus be concluded that capacitive LIG sensors being reagentless, fast, and highly sensitive, are readily expandable to biorecognition elements such as antibodies (You et al. 2020), DNA or even for the direct detection of biomarkers(Hui et al. 2019). Furthermore, their simple and inexpensive fabrication procedure easily enables a multiplexed format. We thus believe that the extraordinary LIG capabilities in conjunction with nanoprobes are ideal for the development of electrochemical point-of-care diagnostic tools.

Acknowledgments

Authors sincerely thank Professor Reinhard Rachel and Mr. Marcel Simsek for providing technical help and assistance in SEM measurements and Ms.Vanessa Tomanek for her contributions to developing the CAD liposome model. This work was supported in part by the South Korean Ministry of Trade, Industry, and Energy (Grant no. P0005440), the South Korean Ministry of Environment (Grant no. 201901136), and the German Federal Ministry of Economic Affairs and Energy (Grant no. ZF4104802AW8). The laser-scriber device was made available through a grant by the King Abdullah University of Science and Technology (KAUST).

Table 1

Extrapolated values of the equivalent circuit elements (CPE) from the fitting results for Figure 2(d,e).

LIG IDEs	Rs [Ω]	CPE	
		T [$\times 10^{-6}$ Ω^{-1}. s^{P}]	P
Electrode 1	865.7 (0.69)	117.7 (1.49)	0.703(0.87)
Electrode 2	751.3 (0.92)	61.36 (1.81)	0.737 (0.88)
Electrode 3	768.1 (1.03)	43.30 (2.0)	0.761 (0.89)

Values in brackets indicated the error %

Table 2

Comparison of the LOD obtained with both electrodes for thrombin in the label-free and the labeled format with polymer nanoparticles (PNPs) and liposome (LP), respectively

	In PBS		In serum
LOD (pM)	Smaller	Bigger	Bigger
Th.	0.8	0.85	1.3
Th. with PNPs	0.7	0.78	-
Th. with LPs	0.66	0.12	-

Table 3

Comparison of sensor characteristics in the present work with previously reported literature for thrombin detection

Materials	Method	Analytical range	LOD	Ref.
Graphene nano composite	Impedance spectroscopy	0.3 to 50 nM	0.01 nM	(Wang et al. 2015)
Interdigitated electrodes	Impedance spectroscopy	1 pM-30 nM	1 pM	(Chen et al. 2019)
Aptamer conjugated Au nanoparticles	Impedance spectroscopy	0.1 nM- 30 nM	0.013 nM	(Li et al. 2011)
Au electrode in microfluidic chip	Impedance spectroscopy	0.1-100000 ng/mL	0.1 ng/mL	(Limi et al. 2017)
Hybridization chain reaction	Differential pulse voltammetry	10 fM - 1.0 nM	3.5 fM	(Wang et al. 2017)
LSG electrode	Differential pulse voltammetry	-	1 pM	(Fenzl et al. 2017)

Toehold-mediated strand displacement reaction-based binding	Differential pulse voltammetry	0.05 nM–100 nM	23.6 pM	(Yang et al. 2018)
Cu_2O@aptamer	Impedance spectroscopy	0.1 to 50 ng/mL	0.01 ng/mL	(Zhang et al. 2015)
Pencil graphite electrode	Impedance spectroscopy	-	19 nM	(Eksin et al. 2015)
Liposomes with LIG electrodes	Impedance spectroscopy	0.01 – 1000 nM	0.12 pM	Present work

Figure captions

Figure 1: (a) Step I: Schematic illustration shows the summary of all aptamer immobilization chemistries for the formation of thrombin receptive interface, step II: schematics represent thrombin and thrombin bound to polymer nanoparticles and to liposome for capacitive sensing strategies; (b) an equivalent circuit model considering two arms of an IDE electrode and simplified equivalent circuit model for the overall capacitance of the developed sensor.

Figure 2: SEM images show the morphology of (a) two IDE arms of the fabricated electrodes and its (b) cross-sectional view of the electrode; (c, d) SEM images of polymer nanoparticles and liposomes, inset of each image shows the size distribution of the particles obtained from DLS measurements.

Figure 3: (a-c) Optical image of three different sized IDEs having finger width of 0.2 mm having separation gap of 0.2 mm in each electrode; d) Bode plots (|Z|, ϕ vs f) obtained for the

same three electrodes in 10 mM PBS over a frequency range of 1 MHz to 0.1 Hz, inset shows the digital picture of the three fabricated IDE electrodes; e) complex capacitance plot derived from the impedance measurements shown in figure (d) with each data point expressed as mean ± SD of impedance measurements on four different electrodes.

Figure 4: Nyquist plots (C′ vs. C″) obtained after surface modification procedures on (a) bigger and (b) smaller electrodes for bare IDE (■), 1-PyBA(●), EDC-NHS(▲), aptamer(▼), BSA(◆) and thrombin(◄), each in a 10 mM PBS pH 6.5; (c) hydrodynamic z-average size and (d) ζ-potential of polymeric nanoparticles and liposomes functionalized with aptamer and subsequent modifications with thrombin.

Figure 5: Nyquist capacitive plots observed on smaller (no. 3, (a-c)) and bigger electrodes (no. 1, (d-f)) depicting the increment in real part of capacitance (C′) by the exposure to different thrombin concentrations ranging from 0.01 nM to 1000 nM for (a,d) the label-free format; (b,e) the polymer nanoparticle format; and (c,f) the liposome labeled format, all measured in PBS (10 mM, pH 6.5).

Figure 6: Calibration curve obtained for the developed sensor for both (a) bigger (no. 1) and (b) smaller electrodes (no. 3) showing ΔC at 0.5 Hz measured with respect to the thrombin concentration; (c) Calibration curve for thrombin capacitance sensors obtained at ΔC at 0.5 Hz for various concentrations of thrombin in PBS (Th -PBS) and serum (Th-serum). Data points are expressed as mean ± SD of four replicate measurements and linearly fitted; (d) complex capacitance plots recorded of aptamer□free IDEs (negative control) after incubation in a solution containing 1 μM thrombin for 30 min. NB: all the other functionalization steps were undertaken except incubating the IDE with aptamer probes. (e) Non-faradaic EIS Bode

plots; and (f) corresponding real part of capacitance extrapolated from electrode modified with aptamer as recorded at different time intervals in PBS (10 mM, pH 6.5). Excellent interfacial stability is evident as the relative standard deviation for the capacitance was less than 0.5 %.

References:

Abstiens, K., Fleischmann, D., Gregoritza, M., Goepferich, A.M., 2019. Gold-Tagged Polymeric Nanoparticles with Spatially Controlled Composition for Enhanced Detectability in Biological Environments. ACS Applied Nano Materials 2(2), 917-926.

Berg, W., Hillvärn, B., Arwin, H., Stenberg, M., Lundström, I., 1979. The Isoelectric Point of Thrombin and its Behaviour Compared to Prothrombin at Some Solid Surfaces. Thromb Haemost 42(08), 972-982.

Bin Seo, H., Gu, M.B., 2017. Aptamer-based sandwich-type biosensors. J Biol Eng 11.

Campuzano, S., Yanez-Sedeno, P., Pingarron, J.M., 2019. Tailoring Sensitivity in Electrochemical Nucleic Acid Hybridization Biosensing: Role of Surface Chemistry and Labeling Strategies. Chemelectrochem 6(1), 60-72.

Castiello, F.R., Porter, J., Modarres, P., Tabrizian, M., 2019. Interfacial capacitance immunosensing using interdigitated electrodes: the effect of insulation/immobilization chemistry. Phys Chem Chem Phys 21(28), 15787-15797.

Cecchetto, J., Fernandes, F.C.B., Lopes, R., Bueno, P.R., 2017. The capacitive sensing of NS1 Flavivirus biomarker. Biosens Bioelectron 87, 949-956.

Chen, H.J., Chen, R.L.C., Hsieh, B.C., Hsiao, H.Y., Kung, Y., Hou, Y.T., Cheng, T.J., 2019. Label-free and reagentless capacitive aptasensor for thrombin. Biosens Bioelectron 131, 53-59.

Cheng, C., Wang, S., Wu, J., Yu, Y., Li, R., Eda, S., Chen, J., Feng, G., Lawrie, B., Hu, A., 2016. Bisphenol A Sensors on Polyimide Fabricated by Laser Direct Writing for Onsite River Water Monitoring at Attomolar Concentration. Acs Appl Mater Inter 8(28), 17784-17792.

Cunningham, J.C., Brenes, N.J., Crooks, R.M., 2014. Paper Electrochemical Device for Detection of DNA and Thrombin by Target-Induced Conformational Switching. Anal Chem 86(12), 6166-6170.

Deng, B., Lin, Y.W., Wang, C., Li, F., Wang, Z.X., Zhang, H.Q., Li, X.F., Le, X.C., 2014. Aptamer binding assays for proteins: The thrombin example-A review. Anal Chim Acta 837, 1-15.

Duan, N., Zhang, H., Nie, Y., Wu, S.J., Miao, T.T., Chen, J., Wang, Z.P., 2015. Fluorescence resonance energy transfer-based aptamer biosensors for bisphenol A using lanthanide-doped KGdF4 nanoparticles. Anal Methods-Uk 7(12), 5186-5192.

Edwards, K.A., Wang, Y., Baeumner, A.J., 2010. Aptamer sandwich assays: human alpha-thrombin detection using liposome enhancement. Anal Bioanal Chem 398(6), 2645-2654.

Eksin, E., Erdem, A., Kuruc, A.P., Kayi, H., Ogunc, A., 2015. Impedimetric Aptasensor Based on Disposable Graphite Electrodes Developed for Thrombin Detection. Electroanal 27(12), 2864-2871.

Erturk, G., Lood, R., 2018. Bacteriophages as biorecognition elements in capacitive biosensors: Phage and host bacteria detection. Sensor Actuat B-Chem 258, 535-543.

Esmon, C.T., Lollar, P., 1996. Involvement of thrombin anion-binding exosites 1 and 2 in the activation of factor V and factor VIII. J Biol Chem 271(23), 13882-13887.

Fenzl, C., Hirsch, T., Baeumner, A.J., 2015. Liposomes with High Refractive Index Encapsulants as Tunable Signal Amplification Tools in Surface Plasmon Resonance Spectroscopy. Anal Chem 87(21), 11157-11163.

Fenzl, C., Nayak, P., Hirsch, T., Wolfbeis, O.S., Alshareef, H.N., Baeumner, A.J., 2017. Laser-Scribed Graphene Electrodes for Aptamer-Based Biosensing. ACS Sens 2(5), 616-620.

Fernandes, F.C.B., Goes, M.S., Davis, J.J., Bueno, P.R., 2013. Label free redox capacitive biosensing. Biosens Bioelectron 50, 437-440.

Ge, L., Hong, Q., Li, H., Li, F., 2019a. A laser-induced TiO2-decorated graphene photoelectrode for sensitive photoelectrochemical biosensing. Chem Commun 55(34), 4945-4948.

Ge, L., Hong, Q., Li, H., Liu, C., Li, F., 2019b. Direct-Laser-Writing of Metal Sulfide-Graphene Nanocomposite Photoelectrode toward Sensitive Photoelectrochemical Sensing. Adv Funct Mater 29(38), 1904000.

Grabowska, I., Sharma, N., Vasilescu, A., Iancu, M., Badea, G., Boukherroub, R., Ogale, S., Szunerits, S., 2018. Electrochemical Aptamer-Based Biosensors for the Detection of Cardiac Biomarkers. Acs Omega 3(9), 12010-12018.

Griffiths, K., Dale, C., Hedley, J., Kowal, M.D., Kaner, R.B., Keegan, N., 2014. Laser-scribed graphene presents an opportunity to print a new generation of disposable electrochemical sensors. Nanoscale 6(22), 13613-13622.

Hayashi, Y., Matsuda, R., Maitani, T., Imai, K., Nishimura, W., Ito, K., Maeda, M., 2004. Precision, limit of detection and range of quantitation in competitive ELISA. Anal Chem 76(5), 1295-1301.

He, C., Xu, Z.H., Sun, T., Wang, L., 2014. Sensitive Electrochemical Aptasensor for Thrombin Detection Based on Graphene Served as Platform and Graphene Oxide as Enhancer. Appl Biochem Biotech 172(2), 1018-1026.

Hui, X., Xuan, X., Kim, J., Park, J.Y., 2019. A highly flexible and selective dopamine sensor based on Pt-Au nanoparticle-modified laser-induced graphene. Electrochim Acta 328.

Kuo, Y.C., Lee, C.K., Lin, C.T., 2018. Improving sensitivity of a miniaturized label-free electrochemical biosensor using zigzag electrodes. Biosens Bioelectron 103, 130-137.

Li, L.D., Zhao, H.T., Chen, Z.B., Mu, X.J., Guo, L., 2011. Aptamer biosensor for label-free impedance spectroscopy detection of thrombin based on gold nanoparticles. Sensor Actuat B-Chem 157(1), 189-194.

Li, X.L., Wu, Y.Y., Niu, J.J., Jiang, D.G., Xiao, D., Zhou, C.S., 2019. One-step sensitive thrombin detection based on a nanofibrous sensing platform. J Mater Chem B 7(34), 5161-5169.

Limi, T., Lee, S.Y., Yang, J., Hwang, S.Y., Ahn, Y., 2017. Microfluidic Biochips for Simple Impedimetric Detection of Thrombin Based on Label-free DNA Aptamers. Biochip J 11(2), 109-115.

Mayer, M., Takegami, S., Neumeier, M., Rink, S., Jacobi von Wangelin, A., Schulte, S., Vollmer, M., Griesbeck, A.G., Duerkop, A., Baeumner, A.J., 2018. Electrochemiluminescence Bioassays with a Water-Soluble Luminol Derivative Can Outperform Fluorescence Assays. Angewandte Chemie International Edition 57(2), 408-411.

Meini, N., Farre, C., Chaix, C., Kherrat, R., Dzyadevych, S., Jaffrezic-Renault, N., 2012. A sensitive and selective thrombin impedimetric aptasensor based on tailored aptamers obtained by solid-phase synthesis. Sensor Actuat B-Chem 166, 715-720.

Nayak, P., Kurra, N., Xia, C., Alshareef, H.N., 2016. Highly Efficient Laser Scribed Graphene Electrodes for On-Chip Electrochemical Sensing Applications. Advanced Electronic Materials 2(10), 1600185.

Nguyen, N.V., Yang, C.H., Liu, C.J., Kuo, C.H., Wu, D.C., Jen, C.P., 2018. An Aptamer-Based Capacitive Sensing Platform for Specific Detection of Lung Carcinoma Cells in the Microfluidic Chip. Biosensors (Basel) 8(4).

Ogihara, N., Itou, Y., Sasaki, T., Takeuchi, Y., 2015. Impedance Spectroscopy Characterization of Porous Electrodes under Different Electrode Thickness Using a Symmetric Cell for High-Performance Lithium-Ion Batteries. J Phys Chem C 119(9), 4612-4619.

Randriamahazaka, H., Asaka, K., 2010. Electromechanical Analysis by Means of Complex Capacitance of Bucky-Gel Actuators Based on Single-Walled Carbon Nanotubes and an Ionic Liquid. J Phys Chem C 114(41), 17982-17988.

Sun, A.L., Qi, Q.G., Wang, X.N., Bie, P., 2014. Porous platinum nanotubes labeled with hemin/G-quadruplex based electrochemical aptasensor for sensitive thrombin analysis via the cascade signal amplification. Biosens Bioelectron 57, 16-21.

Sun, D.P., Luo, Z.B., Lu, J., Zhang, S.S., Che, T., Chen, Z.G., Zhang, L.Y., 2019. Electrochemical dual-aptamer-based biosensor for nonenzymatic detection of cardiac troponin I by nanohybrid electrocatalysts labeling combined with DNA nanotetrahedron structure. Biosens Bioelectron 134, 49-56.

Taberna, P.L., Simon, P., Fauvarque, J.F., 2003. Electrochemical characteristics and impedance spectroscopy studies of carbon-carbon supercapacitors. J Electrochem Soc 150(3), A292-A300.

Teeparuksapun, K., Hedstrom, M., Wong, E.Y., Tang, S.X., Hewlett, I.K., Mattiasson, B., 2010. Ultrasensitive Detection of HIV-1 p24 Antigen Using Nanofunctionalized Surfaces in a Capacitive Immunosensor. Anal Chem 82(20), 8406-8411.

Tsouti, V., Boutopoulos, C., Zergioti, I., Chatzandroulis, S., 2011. Capacitive microsystems for biological sensing. Biosens Bioelectron 27(1), 1-11.

Wang, C.Y., Qian, Y., Zhang, Y., Meng, S.Y., Wang, S.Y., Li, Y.H., Gao, F.L., 2017. A novel label-free and signal-on electrochemical aptasensor based on the autonomous assembly of hemin/G-quadruplex and direct electron transfer of hemin. Sensor Actuat B-Chem 238, 434-440.

Wang, Q.Q., Zhou, Z.X., Zhai, Y.L., Zhang, L.L., Hong, W., Zhang, Z.Q., Dong, S.J., 2015. Label-free aptamer biosensor for thrombin detection based on functionalized graphene nanocomposites. Talanta 141, 247-252.

Wolberg, A.S., Campbell, R.A., 2008. Thrombin generation, fibrin clot formation and hemostasis. Transfus Apher Sci 38(1), 15-23.

Xu, G., Jarjes, Z.A., Wang, H.-W., Phillips, A.R.J., Kilmartin, P.A., Travas-Sejdic, J., 2018. Detection of Neurotransmitters by Three-Dimensional Laser-Scribed Graphene Grass Electrodes. Acs Appl Mater Inter 10(49), 42136-42145.

Yagati, A.K., Park, J., Cho, S., 2016. Reduced Graphene Oxide Modified the Interdigitated Chain Electrode for an Insulin Sensor. Sensors-Basel 16(1).

Yang, J.M., Wu, Y.A., Gan, C.F., Yuan, R., Xiang, Y., 2018. Target-programmed and autonomous proximity binding aptasensor for amplified electronic detection of thrombin. Biosens Bioelectron 117, 743-747.

You, Z., Qiu, Q., Chen, H., Feng, Y., Wang, X., Wang, Y., Ying, Y., 2020. Laser-induced noble metal nanoparticle-graphene composites enabled flexible biosensor for pathogen detection. Biosens Bioelectron 150, 111896.

Zhang, Z.H., Zhang, S., Liu, S.L., Wang, M.H., Fu, G.D., He, L.H., Yang, Y.Q., Fang, S.M., 2015. Electrochemical aptasensor based on one-step synthesis of Cu2O@aptamer nanospheres for sensitive thrombin detection. Sensor Actuat B-Chem 220, 184-191.

Zhao, W.A., Chiuman, W., Brook, M.A., Li, Y.F., 2007. Simple and rapid colorimetric biosensors based on DNA aptamer and noncrosslinking gold nanoparticle aggregation. Chembiochem 8(7), 727-731.

Zhu, Z., Feng, M., Zuo, L., Zhu, Z., Wang, F., Chen, L., Li, J., Shan, G., Luo, S.Z., 2015. An aptamer based surface plasmon resonance biosensor for the detection of ochratoxin A in wine and peanut oil. Biosens Bioelectron 65, 320-326.

a

Step I: Transducer surface

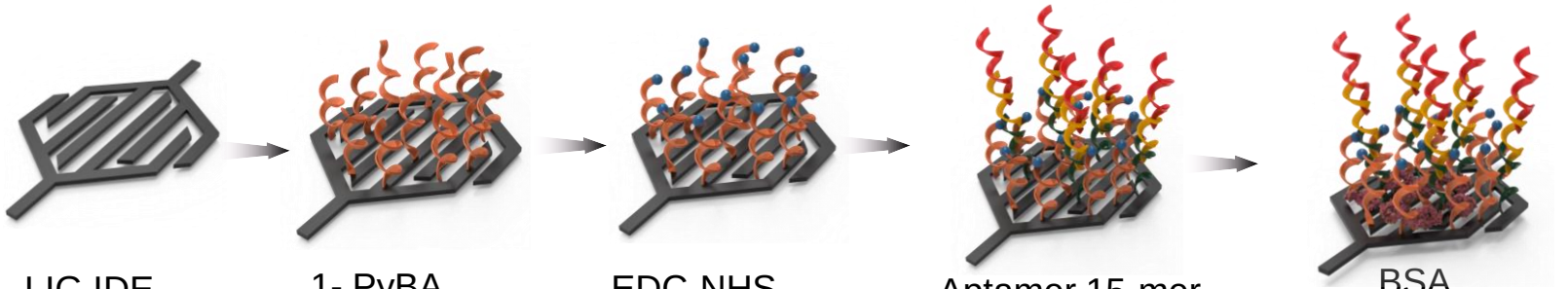

LIG IDE

1- PyBA
10 mM, 90 min

EDC-NHS
50 mM, 45 min

Aptamer 15-mer
10 µM, 3 h

BSA
1 %, 60 min

b

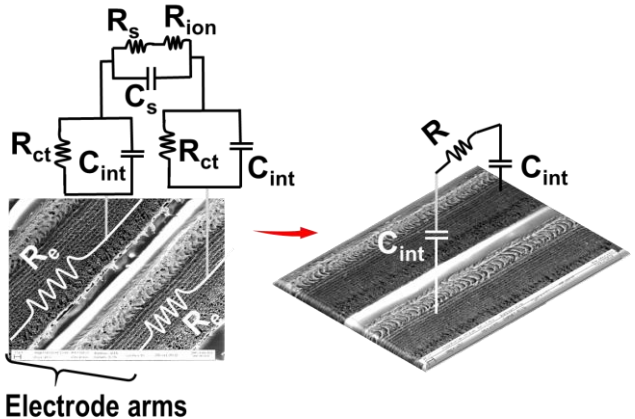

Step II: Analytes and probes

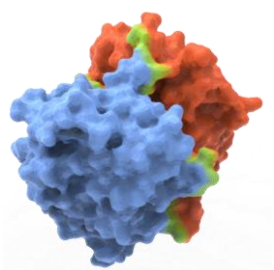

Thrombin

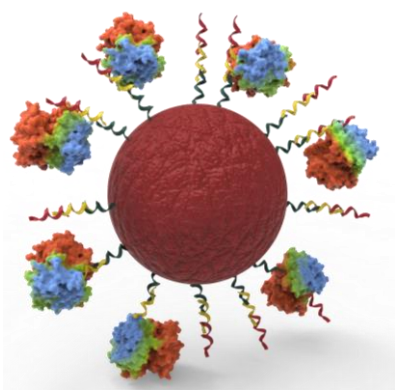

Thrombin bindings
to polymer particle

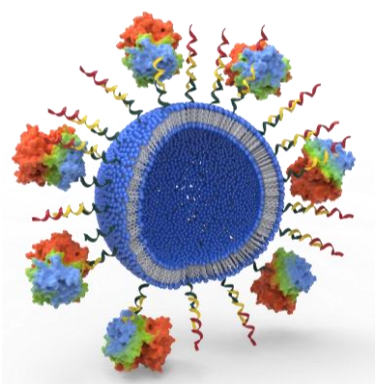

Thrombin bindings
to liposome

$$Z_{\text{LIG IDE}} = R - \frac{1}{j\omega C_{eq}};$$

$$C_{eq} = \frac{C_{int}}{2}$$

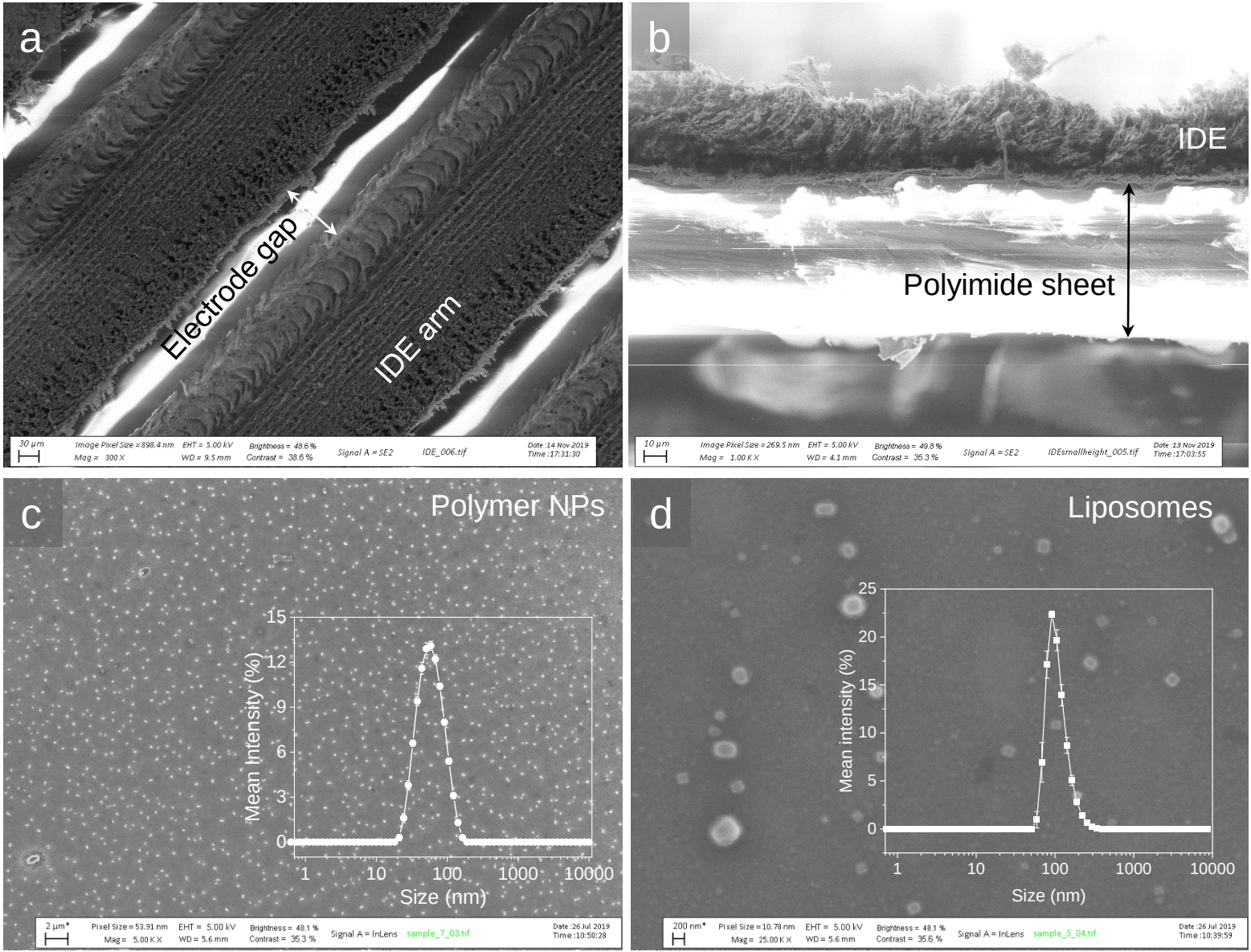
a
Electrode gap
IDE arm
30 µm
Image Pixel Size = 898.4 nm
Mag = 300 X
EHT = 5.00 kV
WD = 9.5 mm
Brightness = 48.6 %
Contrast = 38.6 %
Signal A = SE2
IDE_006.tif
Date :14 Nov 2019
Time :17:31:30
b
IDE
Polyimide sheet
10 µm
Image Pixel Size = 269.5 nm
Mag = 1.00 K X
EHT = 5.00 kV
WD = 4.1 mm
Brightness = 49.8 %
Contrast = 36.3 %
Signal A = SE2
IDEsmallheight_005.tif
Date :19 Nov 2019
Time :17:03:55
c
Polymer NPs
Mean Intensity (%)
0
3
6
9
12
15
1
10
100
1000
10000
Size (nm)
2 µm*
Pixel Size = 53.91 nm
Mag = 5.00 K X
EHT = 5.00 kV
WD = 5.6 mm
Brightness = 48.1 %
Contrast = 35.3 %
Signal A = InLens
sample_7_03.tif
Date :26 Jul 2019
Time :10:50:28
d
Liposomes
Mean intensity (%)
0
5
10
15
20
25
1
10
100
1000
10000
Size (nm)
200 nm*
Pixel Size = 10.78 nm
Mag = 25.00 K X
EHT = 5.00 kV
WD = 5.6 mm
Brightness = 48.1 %
Contrast = 35.6 %
Signal A = InLens
sample_5_04.tif
Date :26 Jul 2019
Time :10:39:59

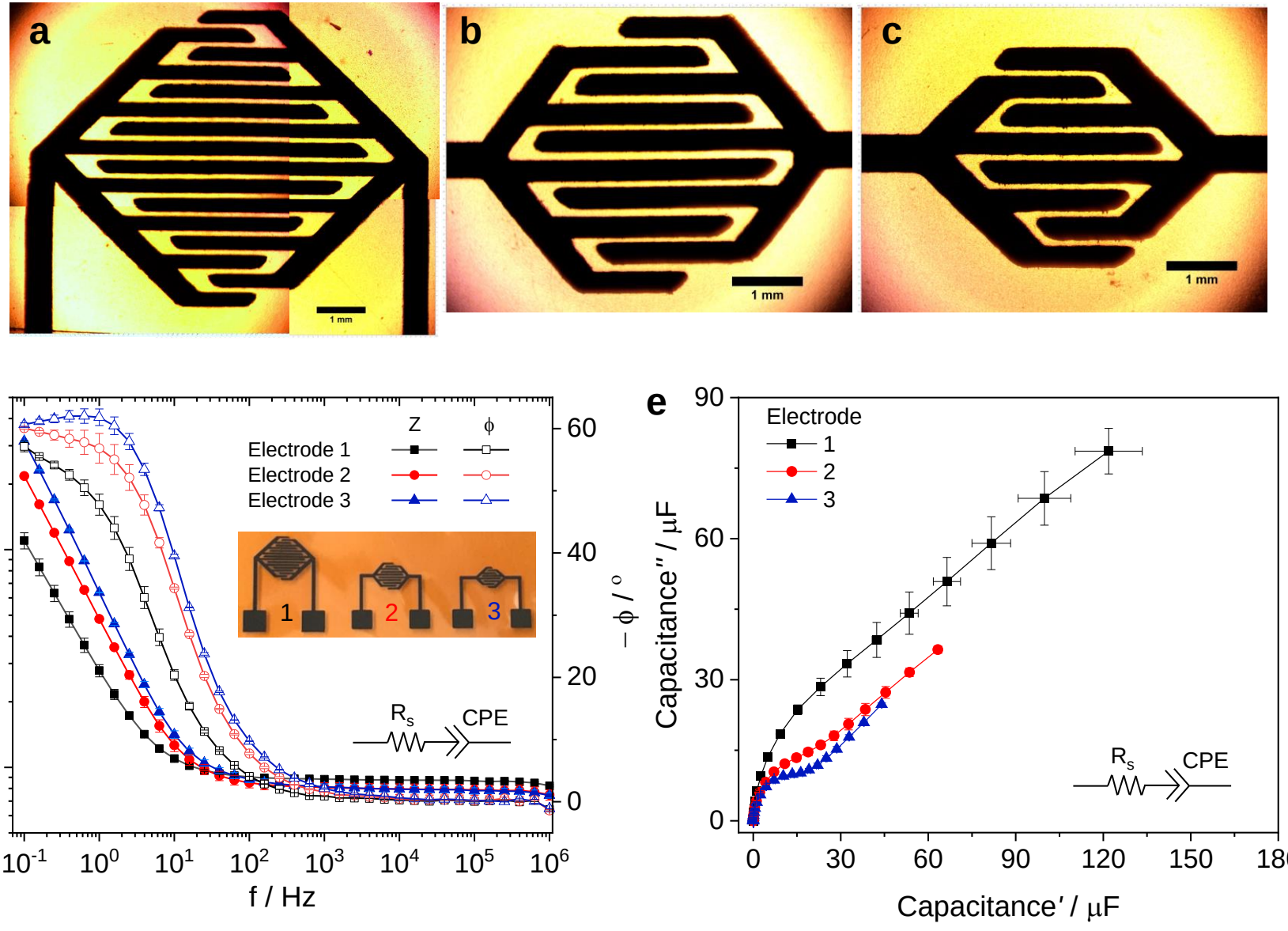
a
b
c
1 mm
1 mm
1 mm
d
Z
ϕ
Electrode 1
Electrode 2
Electrode 3
1
2
3
R_s
CPE
|Z| / Ω
− ϕ / °
f / Hz
e
Electrode
1
2
3
R_s
CPE
Capacitance″ / μF
Capacitance′ / μF

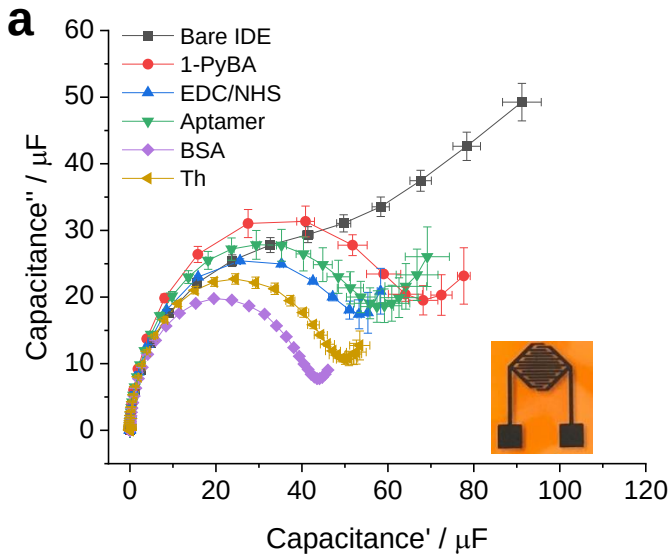
a
Bare IDE
1-PyBA
EDC/NHS
Aptamer
BSA
Th
Capacitance'' / μF
Capacitance' / μF

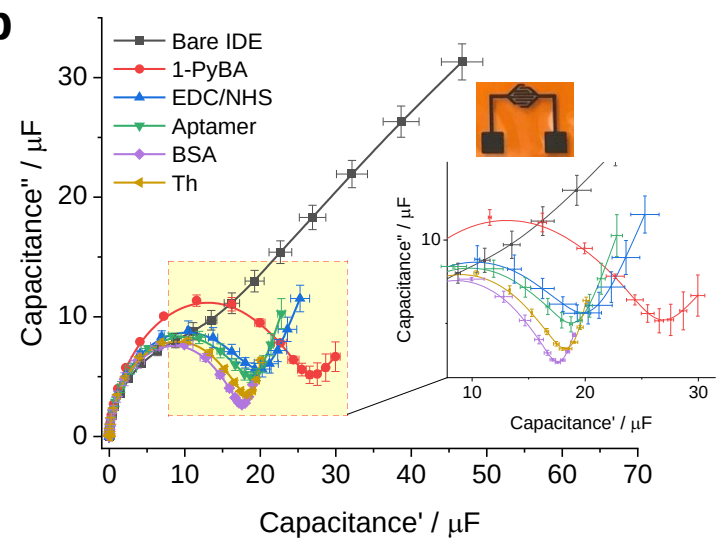
b
Bare IDE
1-PyBA
EDC/NHS
Aptamer
BSA
Th
Capacitance'' / μF
Capacitance' / μF
Capacitance'' / μF
Capacitance' / μF

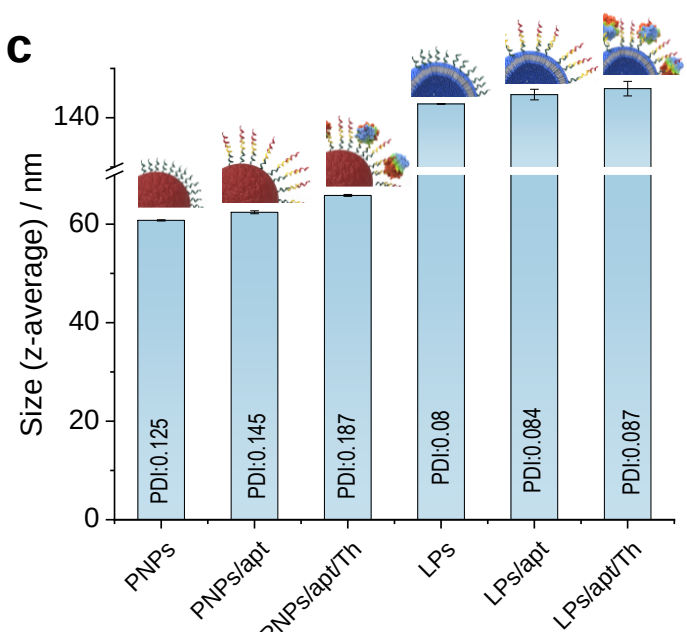
c
Size (z-average) / nm
PDI:0.125
PDI:0.145
PDI:0.187
PDI:0.08
PDI:0.084
PDI:0.087
PNPs
PNPs/apt
PNPs/apt/Th
LPs
LPs/apt
LPs/apt/Th

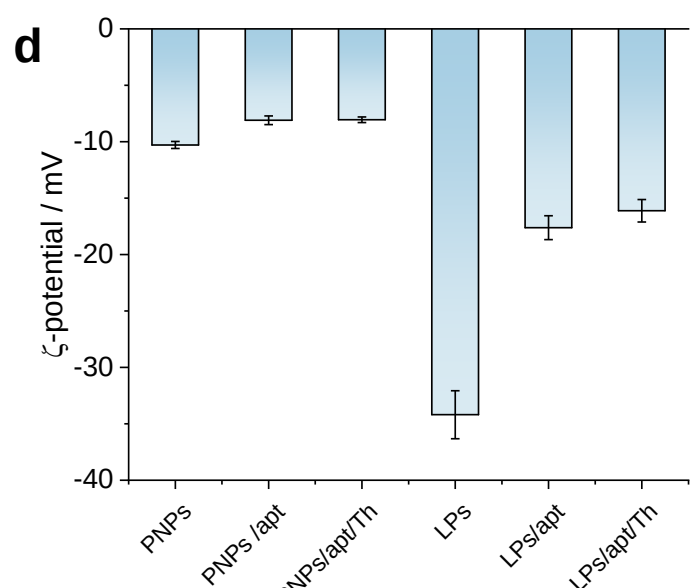
d
ζ-potential / mV
PNPs
PNPs /apt
PNPs/apt/Th
LPs
LPs/apt
LPs/apt/Th

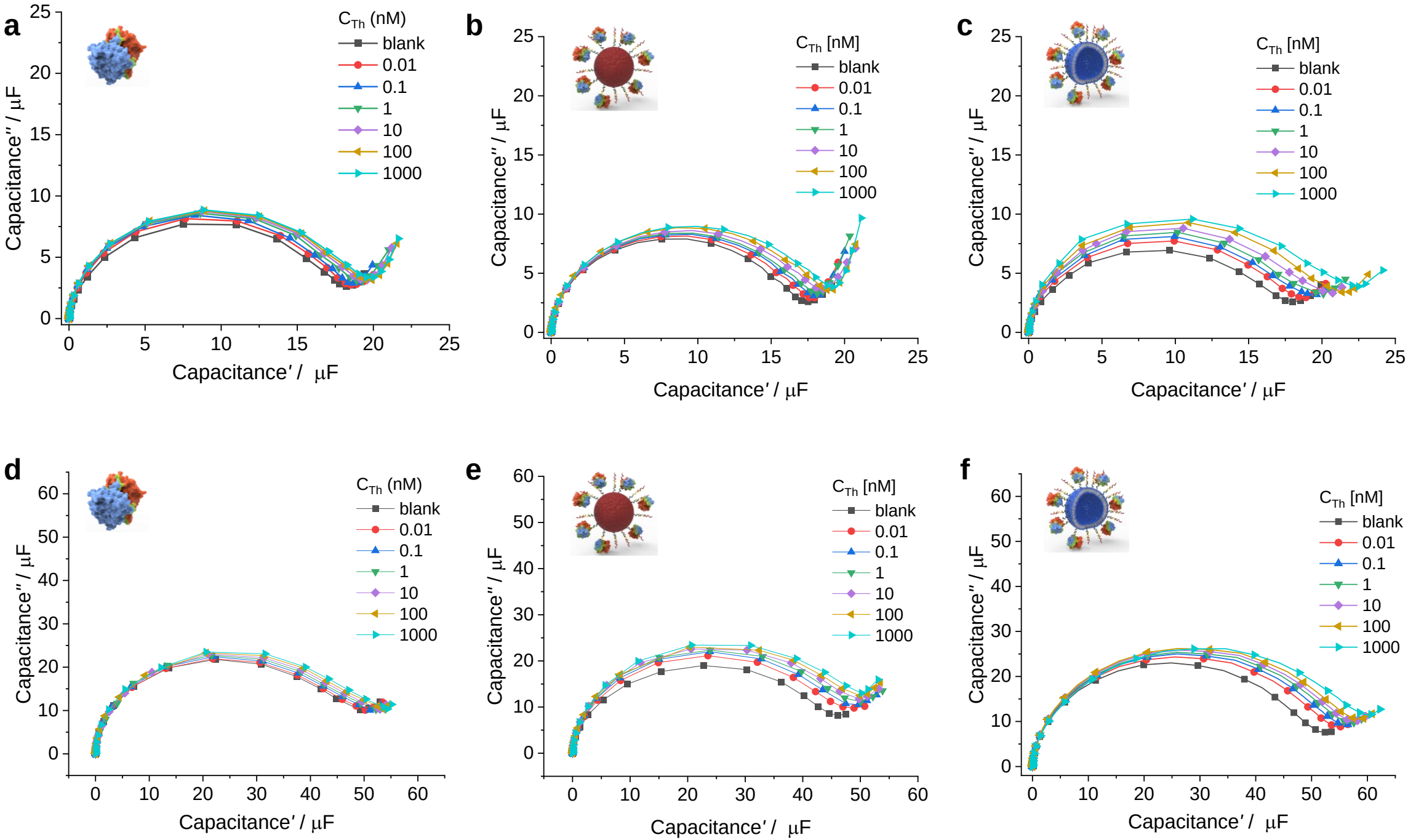
a
b
c
d
e
f
C_Th (nM)
C_Th [nM]
blank
0.01
0.1
1
10
100
1000
Capacitance'' / μF
Capacitance' / μF

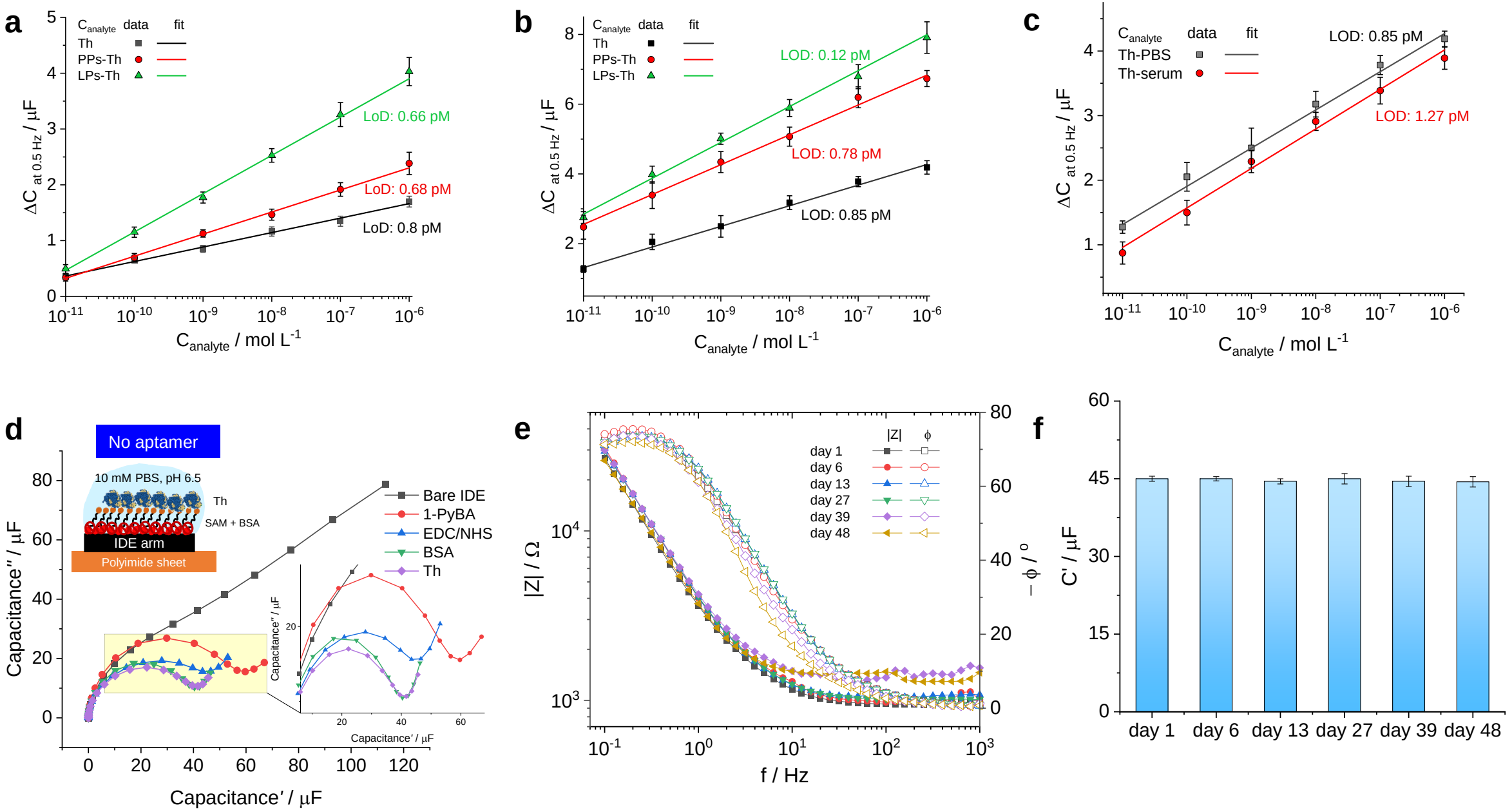
a
C analyte data fit
Th
PPs-Th
LPs-Th
LoD: 0.66 pM
LoD: 0.68 pM
LoD: 0.8 pM
ΔC at 0.5 Hz / μF
C analyte / mol L-1
b
C analyte data fit
Th
PPs-Th
LPs-Th
LOD: 0.12 pM
LOD: 0.78 pM
LOD: 0.85 pM
ΔC at 0.5 Hz / μF
C analyte / mol L-1
c
C analyte data fit
Th-PBS
Th-serum
LOD: 0.85 pM
LOD: 1.27 pM
ΔC at 0.5 Hz / μF
C analyte / mol L-1
d
No aptamer
10 mM PBS, pH 6.5
Th
SAM + BSA
IDE arm
Polyimide sheet
Bare IDE
1-PyBA
EDC/NHS
BSA
Th
Capacitance'' / μF
Capacitance' / μF
e
|Z|
ϕ
day 1
day 6
day 13
day 27
day 39
day 48
|Z| / Ω
– ϕ / °
f / Hz
f
C' / μF
day 1
day 6
day 13
day 27
day 39
day 48

Highlights

Laser-induced graphene interdigitated electrodes for label-free or nanolabel-enhanced highly sensitive capacitive aptamer-based biosensors

- Changes in interfacial capacitance (C_{int}) influenced the overall |Z|, which allowed highly sensitive detection of thrombin on LIG electrodes.
- LIG porous electrodes increased the overall sensitivity of the assay with little contributions from nano-labels needed.
- The sensor possessed an LOD of 0.12 pM with a dynamic range of 0.01 – 1000 nM.
- Sensors showed excellent performance for selective and sensitive detection of thrombin with good reproducibility (RSD, 4.90 %) and repeatability (2.59 %).

Declaration of interests

☒ The authors declare that they have no known competing financial interests or personal relationships that could have appeared to influence the work reported in this paper.

☐The authors declare the following financial interests/personal relationships which may be considered as potential competing interests: